Published in final edited form as:
Cancer Discov. 2011 July 1; 1(2): 144–157. doi:10.1158/2159-8274.CD-11-0010.

Ovarian cancer spheroids use myosin-generated force to clear the mesothelium

Marcin P. Iwanicki[1], **Rachel A. Davidowitz**[1], **Mei Rosa Ng**[1], **Achim Besser**[1], **Taru Muranen**[1], **Melissa Merritt**[2], **Gaudenz Danuser**[1], **Tan Ince**[2,#], and **Joan S. Brugge**[1,*]

[1]Department of Cell Biology, Harvard Medical School, Boston, 02115 MA, USA

[2]Brigham and Women's Hospital, Division of Women's and Perinatal Pathology, Boston, 02115 MA, USA

Abstract

Dissemination of ovarian tumors involves the implantation of cancer spheroids into the mesothelial monolayer on the walls of peritoneal and pleural cavity organs. Biopsies of tumors attached to peritoneal organs show that mesothelial cells are not present under tumor masses. We have developed a live, image-based *in vitro* model in which interactions between tumor spheroids and mesothelial cells can be monitored in real time to provide spatial and temporal understanding of mesothelial clearance. Here we provide evidence that ovarian cancer spheroids utilize integrin – and talin - dependent activation of myosin and traction force to promote mesothelial cells displacement from underneath a tumor cell spheroid. These results suggest that ovarian tumor cell clusters gain access to the sub-mesothelial environment by exerting force on the mesothelial cells lining target organs, driving migration and clearance of the mesothelial cells.

Keywords

ovarian cancer; mesothelium; myosin; integrins; force

INTRODUCTION

During the progression of ovarian cancer, tumor cells detach from the primary tumor site and form cell clusters, or spheroids, that can either remain unattached in the peritoneal cavity or implant onto peritoneal organs (1). Formation of implants depends on the ability of tumor cells to invade into the mesothelial layer that covers peritoneal and pleural organs (2). Electron micrographs of mesothelial tissue sections with and without peritoneal metastases (3, 4) revealed that normal peritoneal mesothelial cells are flat and cover the entire surface of the peritoneum, such that cell-cell boundaries are difficult to discern, whereas, the mesothelial cells with peritoneal metastases are more rounded and separated from each other, revealing the sub-mesothelial surface. These studies suggested that mesothelial cells retracted in the presence of the tumor. Furthermore, the cancer cells did not adhere to the mesothelial cells, but rather to connective tissue under the mesothelial cells. In addition, electron micrographs of excised human peritoneum-associated tumors revealed that mesothelial cells are not present directly under the tumor mass, suggesting mesothelial clearance from the area beneath the tumor mass (4). Early, in vitro, experiments also

Correspondence to: Joan S. Brugge: Harvard Medical School, Department of Cell Biology, Building C, room 513. Boston, MA 02115, Joan_Brugge@hms.haravard.edu.
[#]Current address: Interdisciplinary Stem Cell Institute, University of Miami Miller School of Medicine, Biomedical Research Building 913 1501 NW 10th Ave, Miami, FL 33136

provided evidence that mesothelial cells retract after coming in contact with tumor cells (5, 6). In these studies ovarian cancer cell clusters disrupted mesothelial cell-cell junctions and penetrated matrix under mesothelial cells, suggesting that the integrity of the mesothelial cell monolayer is altered by the attached tumor cells that bind with high affinity to sub-mesothelial matrix, (6, 7). The cellular and molecular mechanisms of mesothelial clearance, however, are unknown.

We have used a live, image-based *in vitro* model in which interactions between tumor spheroids and mesothelial cells can be monitored in real time to provide spatial and temporal understanding of the process of mesothelial clearance. Using this model, we demonstrate that tumor spheroid attachment and spreading on a mesothelial monolayer promotes clearance of the mesothelial cells from the area underneath the spheroid. We provide evidence that force generation on the mesothelial cell-associated extra-cellular matrix provokes mesothelial cells to migrate and clear from underneath the tumor spheroid. This mechanism might be relevant to processes involved in implantation of ovarian tumor aggregates into the sub-mesothelial environment of the organs of the peritoneal and pleural cavities.

RESULTS

Interaction of ovarian cancer spheroids with mesothelial monolayers promotes mesothelial cell clearance

To investigate the interaction between ovarian cancer spheroids (OVCA433 ovarian cancer cell line) and GFP-expressing mesothelial cells (normal immortalized lung mesothelium), we used time-lapse microscopy to follow the dynamics of a mesothelial monolayer after cancer spheroid attachment, in real time. As the spheroid spread on the mesothelial monolayer, mesothelial cells were displaced from the area directly underneath the spreading spheroid. This phenomenon will be referred to as mesothelial clearance. (Figure 1A and Supplementary movie 1). The clearance area increased with time as the spheroid became more incorporated into the mesothelial monolayer (Figure 1B). We also observed that primary tumor clusters isolated from the peritoneal fluid of ovarian cancer patients are able to attach to and clear the mesothelium (Figure 1C and Supplementary movie 2). Overall, these data indicate that, following attachment to a mesothelial monolayer, clusters of ovarian cancer cells are able to induce clearance of the mesothelial cells directly underneath the tumor spheroid.

In vivo, mesothelial cells are separated from the underlying soft connective tissue by a layer of matrix (8). To examine whether mesothelial clearance can occur on more physiologically relevant substrates (of similar stiffness to connective tissue), mesothelial monolayers were plated on fibronectin-coated polyacrylamide gels with elastic moduli of 0.3 kPa or 10kPa. OVCA433 tumor spheroids were able to induce mesothelial clearance on both substrates (Supplementary Figure 1A), indicating that mesothelial clearance can indeed occur on softer, more physiologically relevant substrates, and that the mesothelial clearance observed is not an artifact of cells grown on stiff glass surfaces.

To study the spheroid-mesothelial interaction more closely, we imaged a spheroid during the process of intercalation into a mesothelial monolayer in multiple focal planes and reconstructed the x-z planes to observe ovarian-mesothelial cell interactions at the ventral and dorsal cell surfaces. In the early stages of clearance (as shown in figure 1D and Supplementary movie 3), cancer cells spread on top of the monolayer (as indicated by the arrows) and then penetrated under the mesothelium (as indicated by *). From these observations, we hypothesized that cancer spheroids adhere to the mesothelial monolayer

and induce localized de-adhesion of the mesothelial cells to ultimately prompt movement of the mesothelial cells away from the spheroid.

To examine whether localized de-adhesion of mesothelial cell matrix adhesions indeed occurs upon contact with a tumor spheroid, we used Total Internal Reflection Fluorescent Microscopy (TIRFM) to monitor mesothelial cell adhesions labeled with paxillin-GFP (this protein localizes to integrin-matrix engagement sites in multiple cell types). TIRFM allows for the visualization of florescent molecules present within 100nm above the surface of the cover slip, thereby minimizing background intensity from cytoplasm. We observed that cancer spheroids (labeled with RFP-actin) approached the mesothelial cell's adhesions (GFP) and promoted matrix adhesion disassembly (Figure 2A and Supplementary movie 4A and 4B). Furthermore, there was little adhesion assembly within the area of contact. In contrast, mesothelial cell matrix adhesions that were not in contact with a tumor spheroid displayed spontaneous adhesion assembly and disassembly events (Figure 2B and Supplementary movie 5). In a separate experiment, we labeled approximately one in 500 mesothelial cells with GFP to track the movement of individual mesothelial cells and observed that mesothelial cells that contacted a cancer spheroid migrated significantly longer distances than the mesothelial cells that did not contact a cancer spheroid (Figure 2C,D and Supplementary movie 6). Overall, our results are consistent with the hypothesis that ovarian cancer spheroids can attach to a mesothelial monolayer, intercalate into the monolayer, and trigger mesothelial cell matrix adhesion disassembly and migration, ultimately leading to mesothelial clearance.

Coupling of myosin contractility to integrins in cancer spheroids is required for mesothelial clearance

Ovarian cancer cell adhesion to a mesothelial monolayer has been shown to involve integrins (9). Cells exert force on the extracellular matrix by coupling myosin contractility to integrins (10) (11). Therefore, we examined whether tumor spheroid expression of myosin II is required to promote mesothelial clearance. OVCA433 cancer spheroids express non-muscle myosin isoforms IIA and IIB (Figure 3A). Both myosin II isoforms were downregulated in OVCA433 cells using small hairpin RNA (shRNA) and small interfering RNA (siRNA) targeting myosin IIA and II B heavy chain respectively (Figure 3A). Myosin heavy chain IIA and IIB attenuation did not prevent the ovarian cancer cells from spreading on surfaces coated with fibronectin and collagen I, indicating that myosin IIA and IIB are not required for spheroid attachment and spreading on fibronectin and collagen coated glass surfaces (Supplementary Figure 1B). However, OVCA433 spheroids with reduced levels of myosin IIA/IIB initiated but were unable to sustain mesothelial clearance (Figure 3B,C and Supplementary movie 7). Attenuation of myosin II in OVCA433 cells by shRNA/siRNA did not prevent adhesion of spheroids to the mesothelial monolayer (Supplementary Figure 1C left panel) or induce apoptosis (Supplementary figure 1C right panel), suggesting that myosin II expression in these cells is dispensable for spheroid attachment. We validated these results with two additional independent shRNA sequences targeting myosin IIA combined with the same siRNA pool for myosin IIB molecules (Supplementary figure 1D). Taken together, these results suggest that OVCA433 cancer spheroids require myosin to induce mesothelial clearance.

The ability of cells to exert force on the outside environment depends on linkage of the actin and myosin network to integrins through recruitment of talin I to adhesion sites (10). We used small hairpin RNA (shRNA) to attenuate the expression of talin I in the spheroids (Figure 3D). Attenuation of talin I expression in OVCA433 spheroids did not induce apoptosis (Supplementary Figure 1C right panel) and had no effect on spreading on glass surfaces coated with fibronectin and collagen I (Supplementary figure 2A). However, decreased expression of talin I but not talin II significantly reduced mesothelial clearance,

even though spheroid adherence to the monolayer was unaffected (Figure 3C, Supplementary movie 8 and Supplementary figure 2B,C). We validated these results with two additional independent shRNA sequences targeting talin I molecule in OVCA433, DOV13 and SKOV3 ovarian cancer cell lines (Supplementary figure 2D). These data indicate that talin I is required for tumor cell interaction and suggest that the linkage of integrins to the actomyosin network in ovarian spheroids contributes to mesothelial clearance.

α5β1 integrin is required for spheroid – induced mesothelial clearance and contributes to the activation of myosin in cancer cells

Because expression of the α_5 integrin fibronectin receptor has been shown to correlate with the development of myosin-driven contractility(12) and increased invasion of ovarian cancer cells (13, 14), we addressed whether α5β1 integrin-mediated activation of contractility contributes to ovarian spheroid–induced mesothelial clearance. First, we blocked the function of α5 integrin in cells that express high levels of α5 integrin (OVCA433 ovarian cancer cells) (Figure 4A). Treatment of OVCA433 cell spheroids, which express high levels of a5 integrin, with α5 integrin blocking antibody significantly decreased spheroid-induced mesothelial clearance (Figure 4B, 4C, Supplementary movie 9). Blocking α5 integrin on DOV13 and SKOV3 spheroids also significantly decreased mesothelial clearance (Supplementary figure 3A).α5 blocking antibodies did not, however, prevent the OVCA433 spheroids from adhering to the mesothelial monolayer (Supplementary movie 8, and Supplementary Figure 3B). Blocking other adhesion receptors expressed by OVCA433 spheroid (data not shown), including CD44 and integrins α_2 and α_v, did not have any significant effect on spheroid-induced mesothelial clearance (Supplementary Figure 3C).

In parallel experiments, we over-expressed α5 integrin in ovarian cancer cells that have a low level of α5 integrin expression (OVCAR5) and are unable to clear a mesothelial monolayer (Supplementary Figure 3D). Ectopic expression of α5 integrin in OVCAR5 cells increased activation of myosin, promoted cell spreading and an increase in stress fibers and other cortical actin contractile structures and increased mesothelial clearance (Figure 4D,E,F and Supplementary movie 10). These results support the hypothesis that α5β1–dependent activation of myosin in ovarian cancer spheroids is required for spheroid-mediated mesothelial clearance.

Cancer spheroids expressing functional α5β1 integrin detach fibronectin fibrils from the surface of the mesothelium

Our data suggests that engagement of the fibronectin receptor α5β1 integrin is an important step in spheroid-induced mesothelial clearance. Fibronectin has been found to be present on the surface of murine mesothelial cells (15). Thus, we addressed whether ovarian cancer spheroids re-organize the fibronectin matrix presented on dorsal surface of the mesothelial monolayer. To determine if fibronectin is organized on the dorsal surface of the mesothelial monolayer, the monolayer was immunostained with an antibody that recognized human fibronectin. We observed that fibronectin fibrils were present on top of the mesothelial monolayer (Figure 5A and Supplementary movie 11). We also detected organized collagen fibers on top of the mesothelium (data not shown); however, blocking the $\alpha_2\beta_1$ integrin collagen receptor did not affect mesothelial clearance (Supplementary Figure 3C). Because fibronectin fibrils contacting the periphery of an intercalated spheroid appeared to be preferentially associated with the spheroid, but not the mesothelial cells (Supplementary movie 11), we investigated whether cancer spheroids detach fibronectin from the mesothelial monolayer. We followed the dynamics of rhodamine-labeled fibronectin organized on top of the mesothelial monolayer in the presence of OVCA433 cancer spheroids. As shown in figure 5B and Supplementary movie 12, cancer spheroids induced

detachment of fibronectin fibrils from the mesothelial cells. As time progressed, some of the fibronectin fibrils organized around the spheroid. In addition, when α5β1 integrin was inhibited by an α5 function blocking antibody, fibronectin did not dissociate from the mesothelial cells, suggesting that dissociation of fibronectin from the top of the mesothelial monolayer was dependent on functional α5β1 integrin expressed by the cancer spheroids (Figure 5C,D). These data suggest that ovarian cancer spheroids utilize α5β1 integrin to dissociate fibronectin from the mesothelial monolayer during clearance.

Cancer cells exert force on a fibronectin-coated substrate in an α5β1 integrin-, talin 1- and myosin-dependent manner

The data presented above show that α5β1 integrin, myosin, and talin are all required in ovarian cancer cells for mesothelial clearance and that α5β1 integrin- dependent binding of the ovarian cancer spheroids to fibronectin organized by the mesothelium is important for the clearance processes. This would suggest that the traction force exerted on the substratum by the spreading spheroids contributes to mesothelial clearance. To determine if modulation of α5, talin I, or myosin affects force generation in the ovarian cancer cells, we used traction force microcopy (16–18). This microscopy technique involves tracking fluorescent beads embedded in the substrate on which cell spread/migrate. Displacement of these beads is used to measure traction force exerted by cells on substrate during spreading/migration. Control OVCAR5 cells, OVCAR5 cells over-expressing α5 integrin, and α5 over-expressing cells treated with either talin I siRNA or blebbistatin were allowed to spread on fibronectin coated polyacrylamide substrates embedded with fluorescently labeled beads. Spreading caused deformation of the substrate, as indicated by the movement of the embedded beads. Tracking the bead displacement and reconstructing the cellular traction stresses allowed us to measure the strain energy invested by the cells to deform the elastic substrate (17). The strain energy can be used as a measure for the contractile strength of cells. As shown in figure 6A, increased expression of α5 integrin in cancer cells correlated with an increase in cellular contractility, as measured by strain energy exerted by the cells. α5 integrin-induced force generation was dependent on myosin activation because treatment of OVCAR5 cells overexpressing α5 integrin with blebbistatin significantly decreased elastic energy exerted on the matrix (Figure 5A). We also observed that downregulation of talin I, but not talin II, in OVCAR5 cells overexpressing α5 integrin decreased force generation on fibronectin substrates (Figure 6B). These results are consistent with a model in which talin I and myosin act downstream of α5 integrin to generate force as ovarian cancer cells interact with fibronectin matrix.

DISCUSSION

In summary, these studies provide new insights into the mechanism whereby ovarian tumor spheroids induce mesothelial cell clearance. Clearance-competent tumor spheroids were found to adhere to the dorsal surface of the mesothelial cells and initiate spreading. Protrusions from the spreading cells penetrated underneath the mesothelial cells causing localized breakdown of the mesothelial cell matrix adhesions, and provoked migration of the mesothelial cells. In tumor spheroids, α5β1 integrin, talin I and myosin II were found to be required for spheroid –induced mesothelial clearance. These experiments suggest that ovarian cancer spheroids use actomyosin contractility to exert force via matrix adhesion to the fibronectin organized on the mesothelial monolayer, ultimately leading to mesothelial clearance (see model, Figure 7). The mesothelial clearance we observe in vitro may be relevant in human tumors since it has been shown that mesothelial cells are not present under ovarian tumor masses found attached to the peritoneal tissues.

In contrast to other epithelial tumors that employ hematogenous or lymphatogenous routes to metastasize, ovarian cancer cells predominantly move within the ascites fluid to

metastasize to new sites within the peritoneal cavity(8). The mesothelial monolayer surface provides a variety of ligands to support the attachment of ovarian cancer cells (1). These ligands include hyaluronic acid, mesothelin and extracellular matrix molecules that are able to engage integrins (19–21). Both CD44 and β1-containing integrin dimers have been implicated as receptors that can mediate ovarian cancer cells adherence to the mesothelium. However, function-blocking antibodies directed against β1 integrin or CD44 only partially block ovarian cancer cells adherence to the mesothelial monolayer in short term, in vitro adhesion assays(9), (19, 22). This suggests that multiple ligands and receptors can support ovarian tumor cell adhesion to the mesothelial monolayer and targeting a single molecule will not abrogate cancer cell interaction with mesothelial cells. Consistent with this, we found that blocking CD44 or selected β1 integrin containing integrin heterodimers expressed by OVCA433 spheroids ($\alpha_2\beta_1$, $\alpha_v\beta_3$, $\alpha_5\beta_1$) did not significantly block OVCA433 spheroid attachment to the mesothelium after 10 hours of co-culture. Interestingly, however, our data indicated that interfering with the function of α5β1 integrin alone can significantly decrease OVCA433, DOV13 and SKOV3 spheroid-induced mesothelial clearance over a period of 10 hours (Supplementary Figure 3A,C). As α5β1 integrin is a fibronectin receptor, these results suggest that cancer spheroids can utilize α5β1 to bind to the fibronectin surrounding the mesothelial cells to mediate mesothelial clearance. Supporting this, we found that as a spheroid clears a space in a mesothelial monolayer, the fibronectin fibrils organized on the top of the mesothelial cells are redistributed away from the mesothelial cells and under the spheroid. This process was dependent on functional α5β1 integrin expressed by the cancer spheroids. In addition, we also observed that the expression level of α5β1 integrin in various ovarian cancer cell lines correlated with the ability of these cells to clear the mesothelium (data not shown). However, it is likely that other, $\alpha_5\beta_1$ integrin-independent mechanisms can mediate clearance as well.

Integrins are the major molecules that can transmit traction forces to the outside environment (23). While α_2 integrin binding to collagen I can induce fibril reorganization and transmit traction forces to the ECM in certain contexts(24), OVCAR5 ovarian tumor spheroids that express high levels of α_2, but not α_5 integrin, were unable to clear the mesothelium in our experiments (Supplementary Figure 3C). In addition, blocking α_2 integrin in OVCA433 cells that express both α_2 and α_5 integrin did not prevent mesothelial clearance (Supplementary figure 3C). It is possible that α2 integrin does not transmit sufficient traction force under conditions of adherence to mesothelial cells to induce clearance of the mesothelial cells. The generation of traction force on fibronectin has been shown to involve two steps: First, clustering of $\alpha_5\beta_1$ integrins promotes strong adhesiveness to matrix and second, recruitment of talin I stabilizes and reinforces formed $\alpha_5\beta_1$ adhesions (25) promoting the exertion of traction force on the matrix force. Our study indicated that the interaction between fibronectin receptor $\alpha_5\beta_1$ integrin expressed by tumor cells and mesothelial-associated fibronectin is a molecular event that contributes to the clearance process. In addition, we show that expression of talin I by tumor spheroids is required for $\alpha_5\beta_1$ -mediated formation of traction force and mesothelial clearance. We found that interfering with the function of another fibronectin receptor, $\alpha_v\beta_3$ integrin, did not affect spheroid–induced mesothelial clearance (Suplementary Figure 3C), suggesting that these receptors do not contribute to development of myosin contractility by OVCA433 spheroids that adhered to the mesothelial monolayer. This is consistent with previous experiments implicating $\alpha_5\beta_1$ but not $\alpha_v\beta_3$ integrins, in the development of contractility (26–28). Our data as well as earlier findings(3) show that the mesothelial cells retract in response to cancer cluster attachment. This raises an interesting question: how does the tumor induce retraction in the mesothelial cells? One possibility is that retraction is induced by the physical force of the spreading tumor cells pulling on the mesothelial cell's associated ECM and provoking mesothelial cells migration away from the spheroid. Alternatively, the retraction of mesothelial cells could be provoked by a repulsive ligand presented on the

tumor cells. In this study, we have shown that force produced by a spreading ovarian cancer cell cluster, via $\alpha_5\beta_1$ integrin, myosin II and talin I, is important for mesothelial clearance. The evidence that ovarian cancer spheroids deficient in non-muscle myosin II were unable to sustain mesothelial clearance suggests that mere contact between tumor cells and mesothelial cells is not sufficient to induce retraction and migration of mesothelial cells and that a repulsive ligand presented by spheroid does not trigger retraction of the mesothelial cells. However, it is possible that interfering with myosin function also perturbs expression or activity of repulsive ligands present on tumor cell plasma membrane. Spheroid-induced mesothelial clearance was accompanied by disassembly of mesothelial cell matrix adhesion sites, indicating that force induced on the mesothelium by cancer spheroids initiates migratory response in individual mesothelial cells. In spheroid-induced matrix adhesion turnover experiments mesothelial cells that originated from peritoneal wall (LP9) exhibited much more dynamic integrin adhesion when compared to mesothelium isolated from lungs (MET5A) (compare movie 4A and 4B). This suggests that mesothelial cells covering different organs might elicit distinct migratory responses when contacting tumor spheroids.

Earlier studies implicated mesothelial apoptosis as a mechanism of clearance as result of tumor cluster attachment (29). In our assays clearance of the mesothelium started about 30 minutes after spheroid attachment and was accompanied by migration of individual mesothelial cells from underneath of tumor spheroid. This observation argues that in our assay mesothelial cells respond to contacting tumor cells by activating migratory, but not apoptotic pathways. However it is possible that mesothelial cells that are “stuck” underneath the spheroid and cannot escape, undergo apoptosis.

In patients with advanced disease ovarian tumor clusters predominantly implant into mesothelial lining of peritoneal cavity-associated organs. Invasive tumor implants are able to cross mesothelial layer and gain access to stroma beneath mesothelium (30). These observations suggest that the mesothelium presents a functional barrier to the spread and progression of ovarian tumors. Hence, one would expect that progression toward invasive disease would be associated with alterations that enable the tumor cells to adhere to the mesothelium and brake mesothelial barrier by provoking mesothelial clearance. Our studies suggest that integrin-dependent activation of myosin contractility in tumor cells is required to perturb the mesothelial barrier. Therefore, our results suggest that acquisition of contractile phenotypes in ovarian tumor cells represents a step towards malignant progression.

MATERIALS AND METHODS

Cell Culture

All cells used in this study were cultured in a 1:1 ratio of Medium 199 (GIBCO) and MCDB 105 (Cell Applications, INC) supplemented with 10% fetal bovine serum (GIBCO). Normal lung mesothelial cells were obtained from a benign pleural effusion from a patient with pneumothorax. These cells were immortalized by simultaneous inactivation of p53 and Rb through ectopic expression of SV40 T antigen and overexpression of human telomerase (fused to GFP) as described previously (31, 32). In experiments involving a mixture of labeled and unlabeled mesothelial cells MET5A (human mesothelioma cells -ATTC) were used as a source of unlabeled cells. In focal adhesion tracking experiments, LP9s, a peritoneum-derived mesothelial cell line (Coriell Cell Repositories) was used. Primary lung mesothelial cells were under passage 20. LP9 cells were used as passage under 10. MET5A mesothelial cells were used under passage 10 and these cells morphologically resembled primary lung mesothelilal cells that we used during the course of this experiment. OVCA433 and OVCAR5 ovarian cancer cell lines were a generous gift from Dr. Dennis Slamon (University of California, Los Angeles).

Spheroid-induced mesothelial clearance assay—The mesothelial cells were plated on glass-bottom dishes (Mat-TEK Corporation) coated with 5ug/ml of fibronectin (Sigma, USA) and/or collagen I (Sigma, USA). Cells were maintained in culture until confluent (48 hrs after plating). To generate spheroids, cells were dissociated by trypsinization, labeled with CMTX-red membrane dye (Molecular Probes), washed 2x with PBS, re-suspended in culture medium and plated on Poly-Hema-coated culture dishes (33). Spheroids were collected for experiments 36–48 hrs later. The cell number varied from 100 to 500 cells per spheroid. OVCAR5 spheroids were generated in the presence of 10ug/ml of soluble bovine fibronectin to increase spheroid cohesion (34, 35). In co-culture experiments, spheroids were added to a confluent mesothelial monolayer, allowed to attach for 60 minutes, and imaged for the indicated time. Only spheroids that remained attached during the experiment were used for quantification.

Fibronectin labeling of mesothelial cells and quantification of fibronectin dissociation

20 ug of rhodamine conjugated fibronectin (Cytoskeleton, USA) was added for a period of 24 hrs to a confluent monolayer of human lung mesothelial cells expressing GFP. To quantify fibronectin dissociation from the top of the mesothelial monolayer in the presence of cancer spheroids, we divided total fluorescent intensity of the fibronectin present beneath the cancer spheroid by the total intensity of GFP labeled mesothelial cells.

Western blots and antibodies

Cells were lysed in 100 μl of RIPA buffer (50 mM HEPESpH 7.4, 1% Triton X-100, 1% sodium deoxycholate, 0.1% SDS, 0.1M NaCl, 1 mM sodium orthovanadate, 0.1 M sodium pyrophosphate,100 mM NaF and 1 mM PMSF). Lysates were clarified by centrifugationat 13,000 ***g*** for 10 minutes. Clarified lysates were boiled in1x sample buffer (0.04 M Tris-HCl pH 6.8, 1% SDS, 1% β-mercaptoethanoland 10% glycerol) for 10 minutes and resolved by SDS-PAGE. Proteinswere transferred to Immobilon membranes (Whatman) and blocked with 5% BSA in PBS (140 mM NaCl, 0.27 mM KCl, 0.43 mM $Na_2HPO_4{\cdot}7H_2O$,0.14 mM KH_2PO_4 pH 7.3), 0.1% Tween 20, pH 7.2 for 1 hour atroom temperature. Membranes were incubated overnight at 4°C with one of the following antibodies: anti-talin I polyclonal antibody (Cell Signalling, 1:1000), anti-actin monoclonal antibody (Sigma, 1:1000), anti-myosin heavy chain IIA polyclonal antibody (Covance, 1:1000), anti-myosin heavy chain IIB polyclonal antibody (1:1000, Covance), anti-filamin Apolyclonal antibody (1:1000, Cell Signaling), anti –cleaved caspase -3 polyclonal antibody (1:1000, Cell Signaling) anti-α5 integrin polyclonal antibody (1:1000, Cell Signaling), anti-phosphorylated myosin light chain serine 18 polyclonal antibody (1:1000, Cell Signaling), or anti-myosin light chain polyclonal antibody (1:1000, Cell Signaling). Membranes were subsequently probed with secondary antibodies linked to horserasish peroxidase (HRP; Santa Cruz). Western blot membranes were developed using enhanced chemiluminescent substrate for detection of HRP (VWR). Western blot results were visualized using kodak film developer and an Epson 3000 scanner. OVCA433 spheroids were treated for 45 min in the presence of low serum medium (OPTIMEM) with the following cell adhesion blocking antibodies: anti- α5β1 (5ug/ml, BD Biosciences), anti-α2β1 (5ug/ml, BD Biosciences) integrins, anti-CD44 (5ug/ml, Sigma). We used non specific serum IgG (10ug/ml, Sigma) in function blocking experiments. Treated spheroids were washed twice with PBS (CellGrow), re-suspended in culture medium and added to the mesothelial monolayer.

shRNAs, siRNAs, cDNA plasmids and reagents

To attenuate the expression level of talin 1 and non-muscle myosin heavy chain IIA, OVCA433 cells were infected with lentiviruses lacking an shRNA sequence (pLKO) as a control, or plasmid containing talin 1 (OpenBiosystems)

(seq#1:CCGGGCAGTGAAAGATGTAGCCAAACTCGAGTTTGGCTACATCTTTC ACTGCTTTTTG

seq#2:CCGGGCCTCAGATAATCTGGTGAAACTCGAGTTTCACCAGATTATCT GAGGCTTTTTG

seq#3:CCGGCGCATTGGCATCACCAATCATCTCGAGATGATTGGTGATGCCA ATGCGTTTTTG) or non-muscle myosin IIA shRNA sequences (OpenBiosystems)

seq#1:CCGGCGCATCAACTTTGATGTCAATCTCGAGATTGACATCAAAGTTG ATGCGTTTTTG

seq#2:CCGGCGCATCAACTTTGATGTCAATCTCGAGATTGACATCAAAGTTG ATGCGTTTTT

seq#3:CCGGGACAGCAATCTGTACCGCATTCTCGAGAATGCGGTACAGATTG CTGTCTTTTT).

Lentivirus-infected cells were selected for 72 hours in medium containing 1ug/ml of puromycin (Dulbecco). To attenuate the expression level of non-muscle myosin IIB in OVCAR433 cells or talin 1 in OVCAR5 cells, we also used a pool of siRNA oligonucleotides against NMIIB or talin 1 respectively (Dharmacon). To ectopically express α5 integrin in OVCAR5 cells, we used a retroviral vector (pLZRS) encoding the human α5 integrin gene (generous gift from Dr.Erik Danen, The Netherlands Cancer Institute). Infected cells were selected in growth medium containing 600ug/ml G418 (Dulbecco). Staurosporin was purchased from CalBiochem (USA).

Live cell imaging

Spheroid-induced mesothelial clearance assay—Imaging was performed using a Nikon Ti-E Inverted Motorized Widefield Fluorescence Microscope with integrated Perfect Focus System and low (20×−0.75 NA) magnification/NA DIC optics, Nikon halogen trans illuminator with 0.52 NA LWD condenser, Nikon fast (<100ms switching time) excitation and emission filter wheels, Sutter fast transmitted and epi-fluorescence light path Smart shutters, Nikon linear-encoded motorized stage, Hamamatsu ORCA-AG cooled CCD camera, custom-built microscope incubation chamber with temperature and CO_2 control, Nikon NIS- Elements AR software v3 and TMC vibration-isolation table

Total Internal Reflection Fluorescence (TIRF) analysis—Mesothelial cell adhesion dynamics were visualized using Nikon Ti-E inverted microscope with integrated Perfect Focus System, Nikon 1.49 NA TIRF DIC optics (60x), Nikon halogen trans illuminator with 0.52 NA LWD and 0.85 NA Dry condenser, Nikon dual-port TIRF/Epi illuminator with motorized laser incident angle adjustment and motorized switching between TIRF and epi-illumination, Solamere laser launch with 100mW 491nm, 75mW 561nm and 30mW 640nm solid state lasers with fiber-optic delivery system and 4-channel AOTF, Prior controller, Prior fast excitation and emission filter wheels, Prior fast transmitted and epi-fluorescence light path shutters, Prior linear-encoded motorized stage, Hamamatsu ImagEM 512×512 back-thinned electron multiplying cooled CCD camera, 20/20 Technologies Bionomic Controller/Stage heater insert, Molecular Devices MetaMorph v7.7 and TMC vibration-isolation table

Analysis of the dynamics of rhodamine-labeled fibronectin—Imaging was performed using a Spinning Disk Confocal Microscope: Nikon Ti-E inverted motorized microscope equipped with integrated Perfect Focus System, Nikon Plan Apo 1.4 NA DIC optics (60x), Nikon halogen trans illuminator with 0.52 NA LWD and 0.85 NA Dry condenser, Yokogawa CSU-X1 spinning disk confocal head with internal motorized high

speed emission filter wheel and Spectral Applied Research Borealis modification for increased light throughput and illumination homogeneity, Spectral Applied Research custom laser merge module (LMM-7) with AOTF and 100–200 mW solid state 442nm, 491nm, 515nm, 561nm, and 642 nm lasers, Semrock 405/488/561/647 and 442/514/647 dichroic mirrors, Prior ProScan II controller, Prior NanoScan piezo Z stage insert for high speed z-series, Prior fast transmitted and epi-fluorescence light path shutters, Hamamatsu ORCA-AG cooled CCD camera, custom built 37°C microscope incubator enclosure with 5% CO_2 delivery, Molecular Devices MetaMorph v7.7 and TMC vibration-isolation table.

Quantification of mesothelial clearance and dissociation of fibronectin

To quantify mesothelial clearance, the non-fluorescent area in the GFP mesothelial monolayer was measured over time and divided by the initial area of the cancer spheroid. To quantify the dissociation of fibronectin from the mesothelial cells, the total fluorescence intensity of rhodamine-labeled fibronectin (enclosed within the area of the spheroid) was divided by the total fluorescent intensity of GFP-labeled mesothelial cells beneath the spheroid. Data was plotted as a point distribution using JMP8 statistical software. We used the non-parametric Mann-Whitney t-test to calculate statistical significance.* denotes p=0.05, ** denotes p =0.01, *** denotes p=0.001.

Cancer spheroid adhesion assay

OVCA433 spheroids were co-cultured with mesothelial monolayers for five hours. Spheroids that did not adhere to the monolayer within this time were removed and re-plated on fibronectin and collagen I coated glass bottom dish for 60 minutes, the spheroids were counted. All spheroids that adhered to the mesothelial monolayer were counted. The number of spheroids adhered to the mesothelial monolayer plus the number of spheroids adhered to the matrix-coated dish represented the total number of spheroids. The percentage of spheroids adhered to the mesothelium was calculated by dividing the amount of spheroids attached to the mesothelium by the total number of spheroids (mesothelium + culture dish).

Preparation of Polyacrylamide (PAA) Gel Substrates for Traction Force Microscopy (TFM)

Fibronectin-coated PAA gels containing 0.2um fluorescent microspheres (Invitrogen) were prepared on glass-bottomed dishes as described previously (Wang and Pelham, 1998). In brief, the glass surfaces were incubated with 0.1N NaOH and air dried. The surfaces were then subsequently incubated with 3-aminopropyltrimethoxysilane (Sigma) and 0.5% glutaraldehyde (Sigma), and washed in distilled H_2O between incubations. After drying, a drop of acrylamide/bis-acrylamide solution containing ammonium persulfate (BioRad), tetramethylethylenediamine (TEMED; Sigma) and 0.2um fluorescent microspheres was pipetted onto the modified glass surface. A coverslip was then placed over the droplets to ensure a flat gel surface after polymerization. Fibronectin was coupled to the PAA substrates via the bi-functional crosslinker sulfosuccinimidyl hexanoate (sulfo-SANPAH; Pierce). For traction force measurements of OvCar5 and OvCar5 cells overexpressing α5 integrin, gels with elastic moduli of approximately 10–20kPa were used.

Traction Force Microscopy and Calculations of Traction Forces

Cells on PAA substrates were imaged with a multispectral multimode spinning disk confocal microscope consisting of a Nikon Ti-E inverted motorized microscope equipped with a custom built 37°C microscope incubator enclosure with 5% CO_2 delivery, an integrated Perfect Focus System, a 40× 0.95NA Plan Apo objective, a Yokogawa CSU-X1 spinning disk confocal head with internal motorized high speed emission filter wheel and Spectral Applied Research Borealis modification for increased light throughput and illumination homogeneity, and a Hamamatsu ORCA-AG cooled CCD camera. Images were

acquired with MetaMorph software (MDS Analytical Technologies). Cells were trypsinized with 0.25% trypsin after imaging to obtain an image of unstrained bead positions as reference frames for analyses. Positions of fluorescent beads were extracted from image series and tracked using time-integrated cross-correlation tracking as described previously. Traction forces generated by the cells were determined using custom MatLab programs following the boundary element and Fourier transform traction cytometry methods described by Sabass et al (17). Square image blocks with a template size of 25pixels (= 4.1um) were centered on each reference bead position, identified as intensity maxima in the reference frame. Bead displacements were defined as the x-y-shift that maximizes the cross-correlation score of these image blocks in a corresponding region of the deformed bead image. To minimize false positive template matching, bead displacements with an insignificant maxima in the cross-correlation score function are rejected (36). Traction forces were reconstructed from the measured bead displacements using an implementation of the regularized Fast Fourier Traction Cytometry (FTTC) method (37) provided by (17). For this study we regarded the PAA substrate as isotropic, linear elastic, infinite half-space, and thus applied the Boussinesq Green function. In order to solve the ill-posed inversion problem, we applied zero-order Tikhonov regularization (38). The –6 has been determined using the L-curve method and we used the strain energy *U*, invested by the cell to deform the substrate, as a measure for cellular contractility (37) $U=\frac{1}{2}\int_{\Omega}\vec{T}(\vec{r})\cdot\vec{u}(\vec{r})d\vec{r}$

Here, $\vec{T}$ and $\vec{u}$ denote the measured displacement and reconstructed traction stress, respectively. To avoid possible boundary artifacts introduced by the FTTC algorithm (37) integration was performed over a hand drawn elliptical domain Ω that just covered the whole footprint of the cell. Data was plotted as a point distribution using JMP8 statistical software. We used the non-parametric Mann-Whitney t-test to calculate statistical significance. *-denotes p=0.05 ** - denotes p =0.01 *** - denotes p=0.001.

Supplementary Material

Refer to Web version on PubMed Central for supplementary material.

Acknowledgments

We thank Ghassan Mouneimne and Cheuk Leung for lab meeting discussions and valued input into the direction of this project. We thank Benedikt Sabass and Ulrich Schwarz for providing the regularized FTTC algorithm. We also thank the Nikon Imaging Center at Harvard Medical School for help with light microscopy especially: Jennifer Waters, Wendy Salmon, Lara Petrak and Cassandra Rogers. This study was funded by NIH Grant 5695837 (to M.I) and by Miriam and Sheldon Adelson Research Foundation grant to J.B.

A.B. and G.D were funded by the NIH Grant R01 GM071868 and the Deutsche Forschungsgemeinschaft through fellowship BE4547/1-1.

References

1. Burleson KM, Casey RC, Skubitz KM, Pambuccian SE, Oegema TR Jr, Skubitz AP. Ovarian carcinoma ascites spheroids adhere to extracellular matrix components and mesothelial cell monolayers. Gynecol Oncol. 2004; 93:170–81. [PubMed: 15047232]
2. Burleson KM, Boente MP, Pambuccian SE, Skubitz AP. Disaggregation and invasion of ovarian carcinoma ascites spheroids. J Transl Med. 2006; 4:6. [PubMed: 16433903]
3. Birbeck MS, Wheatley DN. An Electron Microscopic Study of the Invasion of Ascites Tumor Cells into the Abdominal Wall. Cancer Res. 1965; 25:490–7. [PubMed: 14297487]
4. Witz CA, Monotoya-Rodriguez IA, Schenken RS. Whole explants of peritoneum and endometrium: a novel model of the early endometriosis lesion. Fertil Steril. 1999; 71:56–60. [PubMed: 9935116]

5. Niedbala MJ, Crickard K, Bernacki RJ. Interactions of human ovarian tumor cells with human mesothelial cells grown on extracellular matrix. An in vitro model system for studying tumor cell adhesion and invasion. Exp Cell Res. 1985; 160:499–513. [PubMed: 3899694]
6. Kiyasu Y, Kaneshima S, Koga S. Morphogenesis of peritoneal metastasis in human gastric cancer. Cancer Res. 1981; 41:1236–9. [PubMed: 7459864]
7. Koga S, Kudo H, Kiyasu Y, Kaneshima S, Iitsuka Y, Takeuchi T, et al. A scanning electron microscopic study on the peritoneal implantation of ascites hepatoma AH100B cells in rats. Gann. 1980; 71:8–13. [PubMed: 7380138]
8. Lengyel E. Ovarian Cancer Development and Metastasis. Am J Pathol.
9. Strobel T, Cannistra SA. Beta1-integrins partly mediate binding of ovarian cancer cells to peritoneal mesothelium in vitro. Gynecol Oncol. 1999; 73:362–7. [PubMed: 10366461]
10. Bershadsky AD, Balaban NQ, Geiger B. Adhesion-dependent cell mechanosensitivity. Annu Rev Cell Dev Biol. 2003; 19:677–95. [PubMed: 14570586]
11. Zhang X, Jiang G, Cai Y, Monkley SJ, Critchley DR, Sheetz MP. Talin depletion reveals independence of initial cell spreading from integrin activation and traction. Nat Cell Biol. 2008; 10:1062–8. [PubMed: 19160486]
12. Huveneers S, Truong H, Fassler R, Sonnenberg A, Danen EH. Binding of soluble fibronectin to integrin alpha5 beta1 -link to focal adhesion redistribution and contractile shape. J Cell Sci. 2008; 121:2452–62. [PubMed: 18611961]
13. Sawada K, Mitra AK, Radjabi AR, Bhaskar V, Kistner EO, Tretiakova M, et al. Loss of E-cadherin promotes ovarian cancer metastasis viaalpha 5-integrin, which is a therapeutic target. Cancer Res. 2008; 68:2329–39. [PubMed: 18381440]
14. Mitra AK, Sawada K, Tiwari P, Mui K, Gwin K, Lengyel E. Ligand-independent activation of c-Met by fibronectin and alpha(5)beta(1)-integrin regulates ovarian cancer invasion and metastasis. Oncogene.
15. Kenny HA, Kaur S, Coussens LM, Lengyel E. The initial steps of ovarian cancer cell metastasis are mediated by MMP-2 cleavage of vitronectin and fibronectin. J Clin Invest. 2008; 118:1367–79. [PubMed: 18340378]
16. Gardel ML, Sabass B, Ji L, Danuser G, Schwarz US, Waterman CM. Traction stress in focal adhesions correlates biphasically with actin retrograde flow speed. J Cell Biol. 2008; 183:999–1005. [PubMed: 19075110]
17. Sabass B, Gardel ML, Waterman CM, Schwarz US. High resolution traction force microscopy based on experimental and computational advances. Biophys J. 2008; 94:207–20. [PubMed: 17827246]
18. Wang N, Tolic-Norrelykke IM, Chen J, Mijailovich SM, Butler JP, Fredberg JJ, et al. Cell prestress. I. Stiffness and prestress are closely associated in adherent contractile cells. Am J Physiol Cell Physiol. 2002; 282:C606–16. [PubMed: 11832346]
19. Cannistra SA, Kansas GS, Niloff J, DeFranzo B, Kim Y, Ottensmeier C. Binding of ovarian cancer cells to peritoneal mesothelium in vitro is partly mediated by CD44H. Cancer Res. 1993; 53:3830–8. [PubMed: 8339295]
20. Kaneko O, Gong L, Zhang J, Hansen JK, Hassan R, Lee B, et al. A binding domain on mesothelin for CA125/MUC16. J Biol Chem. 2009; 284:3739–49. [PubMed: 19075018]
21. Casey RC, Burleson KM, Skubitz KM, Pambuccian SE, Oegema TR Jr, Ruff LE, et al. Beta 1-integrins regulate the formation and adhesion of ovarian carcinoma multicellular spheroids. Am J Pathol. 2001; 159:2071–80. [PubMed: 11733357]
22. Strobel T, Swanson L, Cannistra SA. In vivo inhibition of CD44 limits intra-abdominal spread of a human ovarian cancer xenograft in nude mice: a novel role for CD44 in the process of peritoneal implantation. Cancer Res. 1997; 57:1228–32. [PubMed: 9102203]
23. Baker EL, Zaman MH. The biomechanical integrin. J Biomech. 43:38–44. [PubMed: 19811786]
24. Friedrichs J, Taubenberger A, Franz CM, Muller DJ. Cellular remodelling of individual collagen fibrils visualized by time-lapse AFM. J Mol Biol. 2007; 372:594–607. [PubMed: 17686490]
25. Roca-Cusachs P, Gauthier NC, Del Rio A, Sheetz MP. Clustering of alpha(5)beta(1) integrins determines adhesion strength whereas alpha(v)beta(3) and talin enable mechanotransduction. Proc Natl Acad Sci U S A. 2009; 106:16245–50. [PubMed: 19805288]

26. Moyano JV, Maqueda A, Casanova B, Garcia-Pardo A. Alpha4beta1 integrin/ligand interaction inhibits alpha5beta1-induced stress fibers and focal adhesions via down-regulation of RhoA and induces melanoma cell migration. Mol Biol Cell. 2003; 14:3699–715. [PubMed: 12972558]
27. Danen EH, Sonneveld P, Brakebusch C, Fassler R, Sonnenberg A. The fibronectin-binding integrins alpha5beta1 and alphavbeta3 differentially modulate RhoA-GTP loading, organization of cell matrix adhesions, and fibronectin fibrillogenesis. J Cell Biol. 2002; 159:1071–86. [PubMed: 12486108]
28. Mierke CT, Frey B, Fellner M, Herrmann M, Fabry B. Integrin {alpha}5{beta}1 facilitates cancer cell invasion through enhanced contractile forces. J Cell Sci. 124:369–83. [PubMed: 21224397]
29. Heath RM, Jayne DG, O'Leary R, Morrison EE, Guillou PJ. Tumour-induced apoptosis in human mesothelial cells: a mechanism of peritoneal invasion by Fas Ligand/Fas interaction. Br J Cancer. 2004; 90:1437–42. [PubMed: 15054468]
30. Seidman JD, Kurman RJ. Ovarian serous borderline tumors: a critical review of the literature with emphasis on prognostic indicators. Hum Pathol. 2000; 31:539–57. [PubMed: 10836293]
31. Hahn WC, Counter CM, Lundberg AS, Beijersbergen RL, Brooks MW, Weinberg RA. Creation of human tumour cells with defined genetic elements. Nature. 1999; 400:464–8. [PubMed: 10440377]
32. Ince TA, Richardson AL, Bell GW, Saitoh M, Godar S, Karnoub AE, et al. Transformation of different human breast epithelial cell types leads to distinct tumor phenotypes. Cancer Cell. 2007; 12:160–70. [PubMed: 17692807]
33. Schafer ZT, Grassian AR, Song L, Jiang Z, Gerhart-Hines Z, Irie HY, et al. Antioxidant and oncogene rescue of metabolic defects caused by loss of matrix attachment. Nature. 2009; 461:109–13. [PubMed: 19693011]
34. Robinson EE, Foty RA, Corbett SA. Fibronectin matrix assembly regulates alpha5beta1-mediated cell cohesion. Mol Biol Cell. 2004; 15:973–81. [PubMed: 14718567]
35. Robinson EE, Zazzali KM, Corbett SA, Foty RA. Alpha5beta1 integrin mediates strong tissue cohesion. J Cell Sci. 2003; 116:377–86. [PubMed: 12482923]
36. Ji L, Danuser G. Tracking quasi-stationary flow of weak fluorescent signals by adaptive multi-frame correlation. J Microsc. 2005; 220:150–67. [PubMed: 16363999]
37. Butler JP, Tolic-Norrelykke IM, Fabry B, Fredberg JJ. Traction fields, moments, and strain energy that cells exert on their surroundings. Am J Physiol Cell Physiol. 2002; 282:C595–605. [PubMed: 11832345]
38. Schwarz US, Balaban NQ, Riveline D, Bershadsky A, Geiger B, Safran SA. Calculation of forces at focal adhesions from elastic substrate data: the effect of localized force and the need for regularization. Biophys J. 2002; 83:1380–94. [PubMed: 12202364]

SIGNIFICANCE

This study employs time-lapse video microscopy to decipher cellular events associated with ovarian tumor cell invasion of mesothelial cell layers. Ovarian cancer clusters used actomyosin generated force to physically displace mesothelial cells and gain access to the sub-mesothelial environment. Blockade of force-conducting molecules including a5 integrin, talin I and non muscle myosin II in cancer cells abrogated mesothelial displacement from underneath attached cancer spheroids.

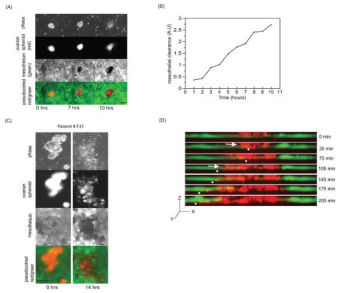

FIGURE 1. Interaction of cancer spheroids with mesothelium prompts mesothelial cell clearance

(A) Ovarian cancer spheroids (OVCA433) labeled with CMTCX cell tracker dye (red) were pipetted on top of a confluent monolayer of GFP-labeled primary TERT immortalized human lung mesothelial cells (green) and incubated for 60 min. The dynamics of these two cell populations were followed in parallel for 10 hours. Images show a time course of mesothelial clearance at 0, 7 and 10 hours. Scale bar = 100μm **(B)** Quantification of mesothelial clearance from experiment shown in A. **(C)** Representative images from a mesothelial clearance assay utilizing a primary tumor cluster isolated from the ascites fluid of an ovarian cancer patient. The sample was labeled and assayed as in *(A)* Scale bar = 50μm. **(D)** Time lapse images of multiple Z sections (side view) of OVCA433 CMTCX-labeled spheroids inducing clearance of GFP- labeled lung mesothelial cells.

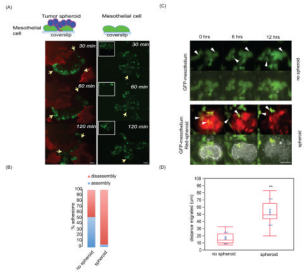

FIGURE 2. Tumor spheroid induces mesothelial cell migration

(A) Temporal analysis of adhesion dynamics of Paxillin-GFP labeled LP9 human peritoneal mesothelial cells incubated with or without RFP-actin expressing OVCA433 cancer spheroids. Events of adhesion assembly and disassembly were scored. Scale bar = 5μm **(B)** The bar graph shows the ratio of adhesion assembly and disassembly events within the same area. A total of *150* assembly and disassembly events were analyzed per condition. **(C)** GFP-labeled lung mesothelial cells were mixed at 1:500 ratio with non -labeled lung mesothelial cells. Images show temporal behavior of single mesothelial cells in the presence or absence of cancer spheroids. Scale bar =100μm **(D)** The migration distance of single mesothelial cells was measured in the presence and absence of OVCA433 cancer spheroids. *50* GFP-labeled mesothelial cells were analyzed per condition.

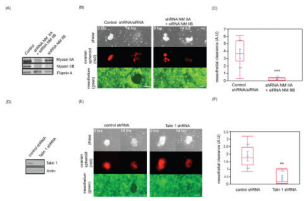

FIGURE 3. Coupling of myosin to integrins in cancer spheroids is required for mesothelial clearance

(A) Western blot of non-muscle myosin heavy chain A and B (NM IIA or NM IIB) expression levels in control or NM IIA/NM IIB shRNA treated OVCA433 cells. **(B)** Images show the temporal behavior of mesothelial cells contacting control or myosin shRNA expressing OVCA433 ovarian cancer cells. Scale bar = 50μm **(C)** Quantification of mesothelial clearance from B. *20* spheroid attachment sites were analyzed per condition. **(D)** Western blot of talin I expression levels in control or talin 1 shRNA expressing OVCA433 cells. **(E)** Images show temporal behavior of mesothelial cells contacting control or talin 1 shRNA expressing OVCA433 ovarian cancer cells. Scale bar = 50μm **(F)** Quantification of mesothelial clearance from E. *15* randomly chosen regions were analyzed per condition.

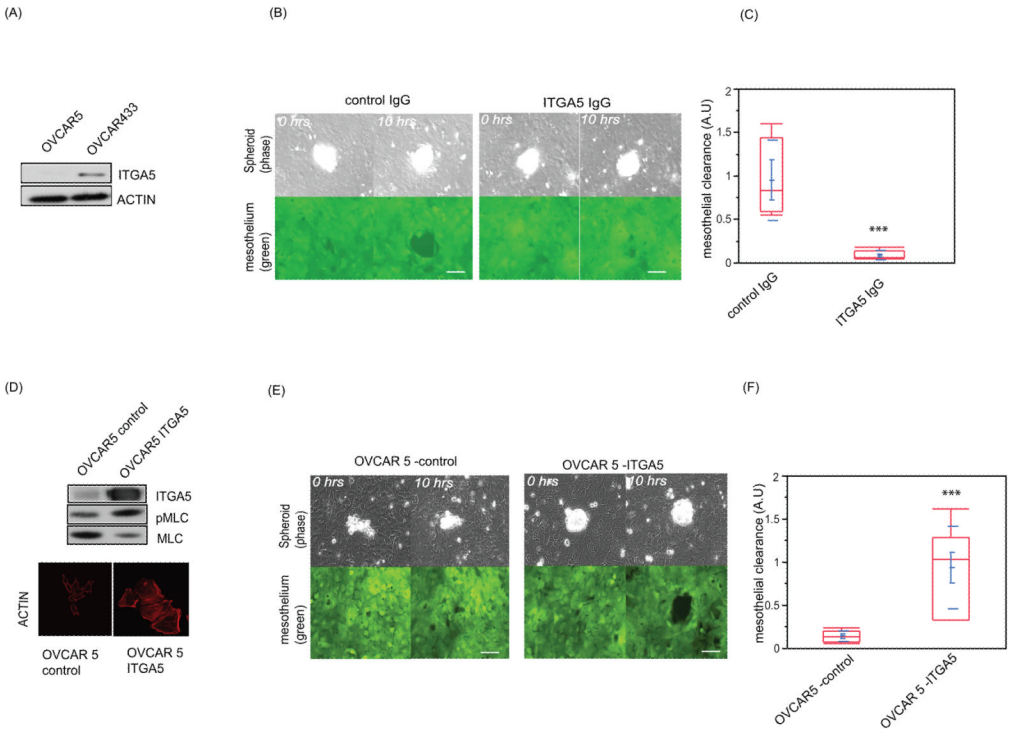

FIGURE 4. α5β1 integrin contributes to the activation of myosin in OVAR5 ovarian cancer cells and is required for OVCAR5 spheroid-induced mesothelial clearance

(A) Western blot analysis of α5 integrin expression levels in OVCAR5 and OVCA433 ovarian cancer cells. Scale Bar = 10μm **(B)** Images depict mesothelial clearance induced by OVCA433 cancer spheroids in the presence of control or α5β1 integrin blocking antibody at 0 and 10 hour time points. Scale bar = 50μm **(C)** Quantification of mesothelial clearance from E. *12* independent regions were analyzed per condition..

(D) Western blot analysis of α5 integrin, phospho-MLC and MLC expression levels in control or α5 overexpressing OVCAR5 ovarian cancer cells plated on fibronectin-coated glass. Images show organization of the actin cytoskeleton in control and α5 integrin overexpressing OVCAR5 ovarian cancer cells plated on fibronectin-coated glass. **(E)** Images represent mesothelial clearance induced by control or α5 integrin overexpressing OVCAR5 cells at 0 and 10 hour time points. Scale bar = 50μm **(F)** Quantification of mesothelial clearance from B. *20* randomly chosen regions were analyzed per condition.

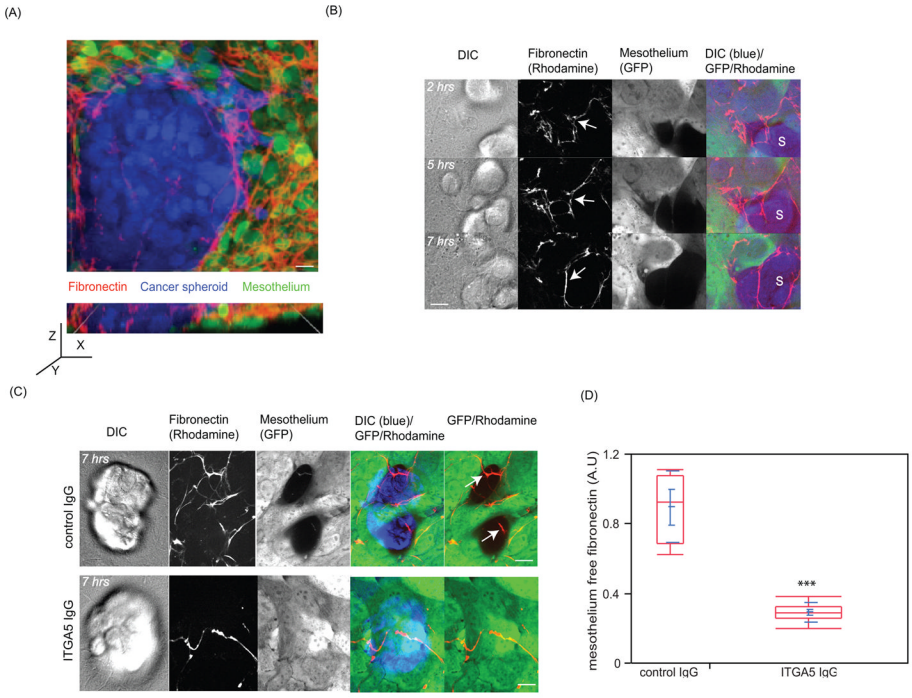

FIGURE 5. Cancer spheroids expressing functional α5β1 integrin dissociate fibronectin fibrils from the surface of the mesothelium

(A) The upper image shows a laser scanning confocal image shows the top view of an OVCA433 cancer spheroid (blue) inserted into a mesothelial monolayer (green) stained with an antibody directed against human fibronectin (red). Scale bar = 10μm. The lower image shows a side view reconstruction of multiple Z planes of the same image. **(B)** Images show temporal acquisition of mesothelium (green) associated fibronectin (red) by OVCA433 cancer spheroids (blue). Scale bar = 10μm **(C)** Dissociation of fibronectin (red) from mesothelial monolayer (green) after 7 hours in response to spheroids (blue) pretreated with either control or α5β1 blocking antibody. Scale bar = 10μm. **(D)** Quantification of fibronectin dissociation from a mesothelial monolayer in response to an attached cancer spheroid pretreated with either control or α5β1 antibody. *8* randomly chosen regions were analyzed in the control group and *20* randomly chosen regions were analyzed in the ITGA5 group.

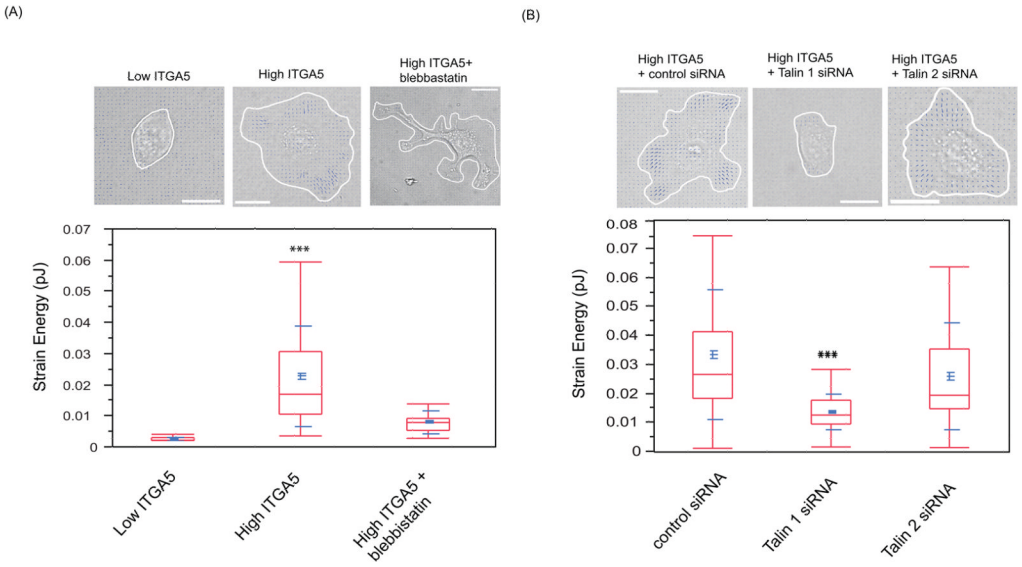

FIGURE 6. Cancer cells exert forces on a fibronectin-coated polyacrylamide gel in an α5β1 integrin, talin 1 and myosin-dependent manner

OVCAR5 ovarian cancer cells were plated on a polyacrylamide (PAA) gel substrate coated with fibronectin (10ug/ml). Cells were allowed to adhere to and spread on the PAA substrate and the displacement of fluorescently labeled beads embedded in the substrate was monitored. The strain energy was calculated from measured bead displacement data and used to reconstruct traction stresses. The strain energy is the energy invested by the cells to deform the substrate and a measure for the overall contractility of a cell (37). **(A)** OVCAR5 cells have low endogenous α5-integrin (ITGA5) expression levels, and are significantly less contractile than OVCAR5 cells overexpressing ITGA5 ($p<0.001$). The high contractility of ITGA5-overexpressing OVCAR5 cells is attenuated by treatment with 1uM blebbistatin ($p<0.001$). **(B)** The contractility of ITGA5-overexpressing OVCAR5 cells can also be significantly attenuated by siRNA-mediated knockdown of Talin 1, but only slightly attenuated by knockdown of Talin II. Bar = 20μm.

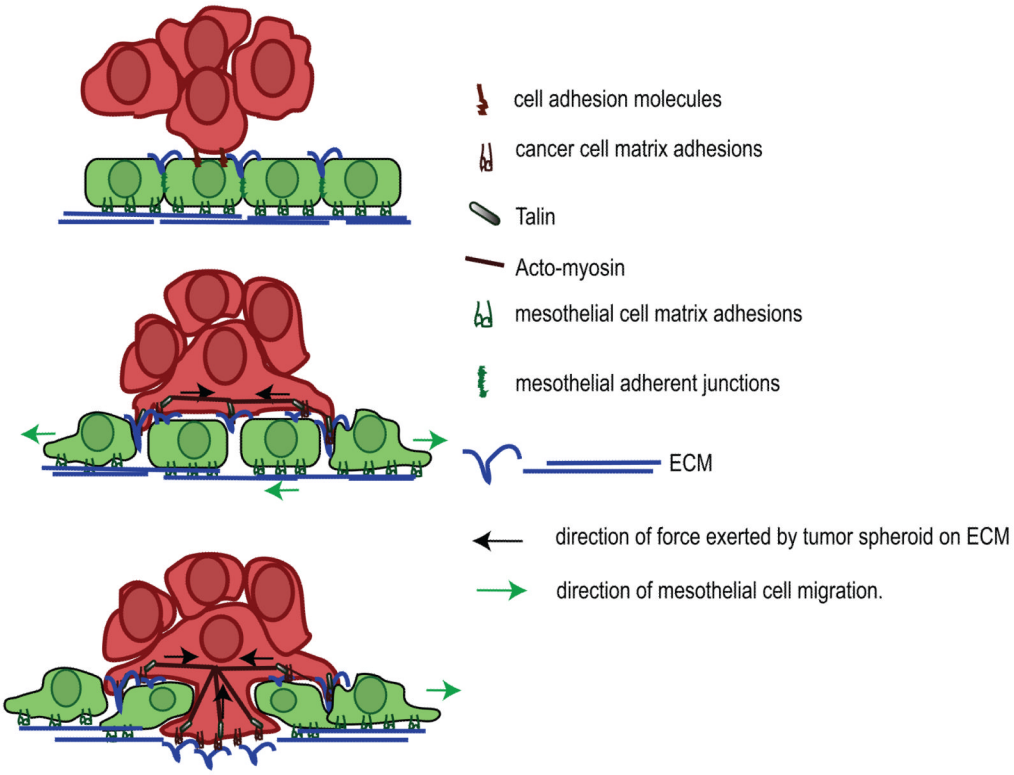

FIGURE 7.

Model depicting the events associated with ovarian tumor cell intercalation into a mesothelial monolayer. Cancer spheroids attach to the mesothelial monolayer using various cell adhesion molecules including CD44,α5β1, αvβ1 and α2β1 integrins. Interaction of α5β1 integrin, expressed on cancer spheroids with fibronectin presented on the mesothelium promotes activation of myosin in the tumor spheroids and transmission of the force from the spheroid to the fibronectin on the monolayer. This promotes dissociation of mesothelial cells adhesions and their migration away form intruding tumor cells, leading to mesothelial cells exclusion from the base of cancer spheroid.